Cell Death & Differentiation (2018) 25:1686–1701
https://doi.org/10.1038/s41418-018-0067-x

Cell Death & Differentiation

ARTICLE

TMCO1 is essential for ovarian follicle development by regulating ER Ca^{2+} store of granulosa cells

Zhongshuai Sun[1] · Hui Zhang[1] · Xi Wang[2] · Qiao-Chu Wang[2] · Chuanchao Zhang[1] · Jiu-Qiang Wang[2] · Yi-Han Wang[2] · Chao-Qiang An[2] · Ke-Yan Yang[2] · Yun Wang[2] · Fei Gao[3] · Caixia Guo[1] · Tie-Shan Tang[2]

Received: 19 July 2017 / Revised: 15 January 2018 / Accepted: 16 January 2018 / Published online: 21 February 2018

Abstract

TMCO1 (transmembrane and coiled-coil domains 1) is an endoplasmic reticulum (ER) transmembrane protein that actively prevents Ca^{2+} stores from overfilling. To characterize its physiological function(s), we generated *Tmco1*$^{-/-}$ knockout (KO) mice. In addition to the main clinical features of human cerebrofaciothoracic (CFT) dysplasia spectrum, *Tmco1*$^{-/-}$ females manifest gradual loss of ovarian follicles, impaired ovarian follicle development, and subfertility with a phenotype analogous to the premature ovarian failure (POF) in women. In line with the role of TMCO1 as a Ca^{2+} load-activated Ca^{2+} channel, we have detected a supernormal Ca^{2+} signaling in *Tmco1*$^{-/-}$ granulosa cells (GCs). Interestingly, although spontaneous Ca^{2+} oscillation pattern was altered, ER Ca^{2+} stores of germinal vesicle (GV) stage oocytes and metaphase II (MII) arrested eggs were normal upon *Tmco1* ablation. Combined with RNA-sequencing analysis, we also detected increased ER stress-mediated apoptosis and enhanced reactive oxygen species (ROS) level in *Tmco1*$^{-/-}$ GCs, indicating the dysfunctions of GCs upon TMCO1 deficiency. Taken together, these results reveal that TMCO1 is essential for ovarian follicle development and female fertility by maintaining ER Ca^{2+} homeostasis of GCs, disruption of which causes ER stress-mediated apoptosis and increased cellular ROS level in GCs and thus leads to impaired ovarian follicle development.

Introduction

Premature ovarian failure (POF) is a heterogeneous and multifactorial disorder, characterized by amenorrhea prior to the age of 40 years and elevated levels of gonadotropins, that is, follicle stimulating hormone (FSH) and luteinizing hormone (LH) [1]. As a most common disease that impairs female fertility, the pathogenical causes of POF were widely studied in human patients with X-chromosome abnormalities [2] and FMR1 (fragile mental retardation 1) CGG expansions [3] as well as in genetically modified mouse models [4–6]. For instance, deletion of *Pten* (phosphatase and tensin homology deleted on chromosome 10) causes over-activation and exhaustion of primordial follicle pool, resulting in POF and subfertility [4].

In mammalian fetal ovaries, primordial germ cells differentiate into primary oocytes and are enclosed by pregranulosa cells to form primordial follicles, the activation of which would start their development to later stage follicles in adult ovaries [7]. Granulosa cells (GCs) provide necessary nutrients and steroids to the oocytes, playing vital roles in ovarian follicle development [8]. Abnormal

These authors contributed equally: Zhongshuai Sun, Hui Zhang, and Xi Wang.

Edited by L Scorrano

These Author's contributed: Zhongshuai Sun,Hui Zhang and Xi Wang equally to this work.

Electronic supplementary material The online version of this article (https://doi.org/10.1038/s41418-018-0067-x) contains supplementary material, which is available to authorized users.

✉ Caixia Guo
guocx@big.ac.cn

✉ Tie-Shan Tang
tangtsh@ioz.ac.cn

[1] Key Laboratory of Genomics and Precision Medicine, Beijing Institute of Genomics, University of Chinese Academy of Sciences, Chinese Academy of Sciences 100101 Beijing China

[2] State Key Laboratory of Membrane Biology, Institute of Zoology, University of Chinese Academy of Sciences, Chinese Academy of Sciences, 100101 Beijing China

[3] State Key Laboratory of Stem Cell and Reproductive Biology, Institute of Zoology, University of Chinese Academy of Sciences, Chinese Academy of Sciences, 100101 Beijing, China

function or apoptosis of GCs has been linked with follicle atresia or deletion [9]. Previous studies have shown that polarity establishment abnormality of GCs causing aberrant follicle development was observed in $Wt1^{+/R394W}$ female mice [10]. Additionally, LGALS3, which is a β-galactoside-binding protein, was increasingly expressed in GC layer of atretic follicles of mouse [11], suggesting *Lgals3* plays an important role in the regression of follicles. Furthermore, downregulated expression of *Inhbb* (*Inhibin βB*) is associated with enhanced apoptosis rate of mouse GCs [12].

TMCO1 (transmembrane and coiled-coil domains 1) is a highly conserved protein localized in the membrane of ER [13]. TMCO1 works as a Ca^{2+} load-activated Ca^{2+} (CLAC) channel to release Ca^{2+} when ER Ca^{2+} is overloaded, thereby maintaining calcium homeostasis [13]. Mutations in the *TMCO1* gene induce an autosomal-recessive TMCO1-defect syndrome, which belongs to human cerebrofaciothoracic (CFT) dysplasia spectrum, characterized by craniofacial and skeletal anomalies and mental retardation [14, 15].

To characterize physiological function(s) of TMCO1, we generated *Tmco1* KO mice that reproduce the main clinical features of human CFT dysplasia spectrum. Unexpectedly, an impaired ovarian follicles development was also manifested in *Tmco1* KO female mice, accompanied with a POF phenotype. In line with the role of TMCO1 as a Ca^{2+} load-activated Ca^{2+} channel, we detected a supernormal Ca^{2+} signaling and overloaded ER Ca^{2+} store in $Tmco1^{-/-}$ GCs. Interestingly, ER Ca^{2+} stores of GV stage oocytes and MII-arrested eggs were normal upon *Tmco1* ablation. Combined with RNA-sequencing analysis and immunoblotting, we further detected an increased ER stress-mediated apoptosis and an enhanced reactive oxygen species (ROS) level in $Tmco1^{-/-}$ GCs, highlighting the important functions of TMCO1 in GCs and ovarian follicle development. Therefore, the normal physiological functions of GCs are critically dependent on the homeostatic maintenance of ER Ca^{2+} store in GCs. Mishandling of ER Ca^{2+} store could be a factor in progressive loss of follicles and eventually POF.

Results

Tmco1 KO female mice display impaired fertility

We previously reported *Tmco1* KO mice generated by TALEN method reproduce the main clinical features of human CFT dysplasia spectrum [13]. Unexpectedly, the loss of developing ovarian follicles was noted in 6-month-old *Tmco1* TALEN KO female mice (Supplementary Figure S1A). To confirm this finding, we generated another $Tmco1^{+/-}$ mouse strain through conventional method, followed by genotype identification through PCR (Supplementary Figures S1B and C). Furthermore, we confirmed that the expression of TMCO1 was completely removed from ovaries, GCs, and GV stage oocytes (Supplementary Figures S1D–F). In line with our previous results, this *Tmco1* KO mouse strain also lacked follicle structure at 6-month-old ovaries, which were smaller and flattened (Supplementary Figure S1K). No ovarian follicles and corpora lutea structures were seen in $Tmco1^{-/-}$ ovaries, except for some cells remnants probably reflecting luteolysis compared with wild-type (WT) ovaries (Supplementary Figures S1G–J).

To evaluate the female mice fertility status, 7-week-old $Tmco1^{+/+}$ and $Tmco1^{-/-}$ female mice were mated with WT males with proven fecundity for nearly 4 months. As shown in Table 1, $Tmco1^{-/-}$ females had fewer numbers of pups per litter. In addition, the total numbers of pups delivered by KO mice were less than half of the control females (315/652). Particularly, more dead pups were born (38/5), leaving only 277 live pups in the KO group (647 in WT). These results suggest $Tmco1^{-/-}$ females were subfertile and declined in productive ability.

Progressive loss of ovarian follicles in $Tmco1^{-/-}$ female ovaries

To understand how TMCO1 loss impairs female fertility, we compared the morphology of ovaries at different age. No apparent morphological changes were observed at postnatal day 2 (PD2, Fig. 1a, b). The germline cyst structure with several oocytes clustered by flattened pregranulosa cells could be noticed in both genotypes (enlargements) and the

Table 1 Fertility assessment of $Tmco1^{+/+}$ and $Tmco1^{-/-}$ female mice

Genotype	Total female mice with plugs	Average no. of pups/litter	Total no. of pups	Total no. of live pups	Total no. of dead pups
$Tmco1^{+/+}$	20	9.258 ± 0.240^{a}	652	647	5
$Tmco1^{-/-}$	20	4.922 ± 0.282^{b}	315	277	38

Female $Tmco1^{+/+}$ and $Tmco1^{-/-}$ 7-week-old mice were mated with WT 2- to 3-month-old C57BL/6J male mice that had proven normal fecundity until the female mice were 6 months old. Female mice with vaginal plug and later visibly growing abdomen were included in this assessment. The numbers of pups per litter or pups (both alive and dead) were assessed. $a > b$, $p < 0.0001$. Data were represented as the mean ± s.e.m.

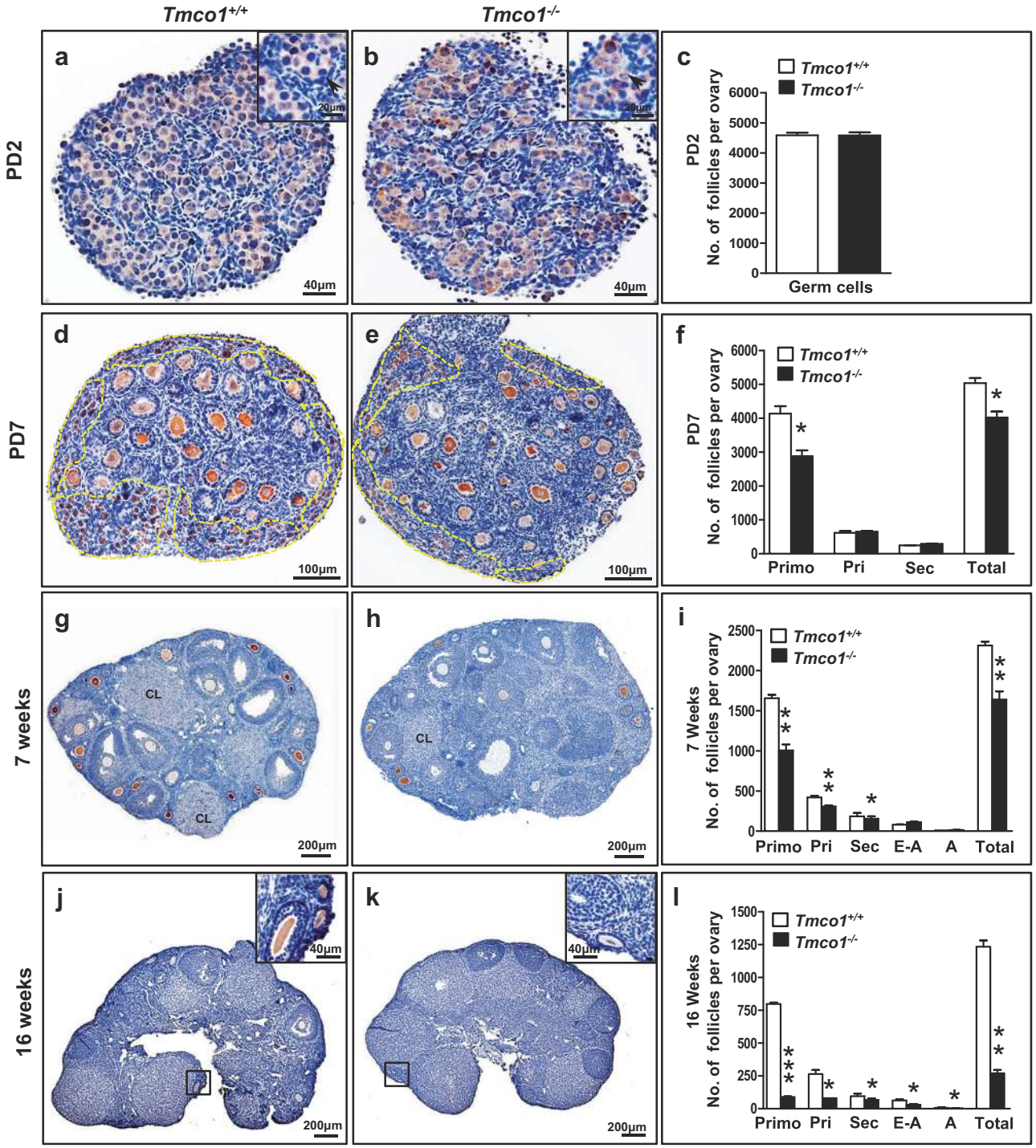

Fig. 1 Ovarian morphologies of PD2, PD7, 7- and 16-week-old *Tmco1* $^{+/+}$ and *Tmco1* $^{-/-}$ mice. MVH antibody was applied in IHC method to manifest oocytes for easier quantification of follicle numbers. At least five mice of each genotype for each time point were measured. Abbreviations: primordial (Primo), primary (Pri), secondary (Sec), early antral (E-A), antral (A), and total (Total) follicles. **a** *Tmco1* $^{+/+}$ and **b***Tmco1* $^{-/-}$ ovaries from PD2 females. Note that germline cyst structure existed in both magnification of the insets in the panel (Scale bar, 20 μm). **c** Quantification of germ cells in PD2 mice. **d***Tmco1* $^{+/+}$ and **e***Tmco1* $^{-/-}$ ovaries from PD7 mice with yellow dot lines indicating primordial follicles. **f** Quantification of follicles at PD7. Primo, $*p = 0.0106$; Total, $*p = 0.0118$. **g** 7-week-old *Tmco1* $^{+/+}$ females and **h** *Tmco1* $^{-/-}$ counterparts. Corpus luteum (CL) structure indicated ovulation had occurred. **i** Statistics summary of follicles at 7 weeks. Primo, $**p = 0.0018$; Pri, $**p = 0.0075$; Sec, $*p = 0.0399$; Total, $**p = 0.0039$. 16-week-old ovarian sections for **j***Tmco1* $^{+/+}$ and **k***Tmco1* $^{-/-}$ mice (magnification of the insets, scale bar, 40 μm). **l** Quantification of follicles in 16-week-old mice. Primo, $***p = 0.0002$; Pri, $*p = 0.0291$; Sec, $*p = 0.0368$; E-A, $*p = 0.0476$; A, $*p = 0.0391$; Total, $**p = 0.0039$. Scale bars, 40 μm (**a**, **b**), 100 μm (**d**, **e**), 200 μm (**g**, **h**, **j**, **k**)

numbers of germ cells were grossly similar (Fig. 1c). However, at PD7, the number of primordial follicles was obviously reduced in KO mice (~3000) compared with WT (~4000, Fig. 1d–f), albeit comparable numbers of primary and secondary follicles were noted, indicating the primordial follicle assembly but not the development transition from primordial follicles to primary and secondary stages was affected in *Tmco1*$^{-/-}$ mice.

In addition, the numbers of primordial, primary, and secondary follicles were significantly decreased in 7-week-old *Tmco1*$^{-/-}$ mice (Fig. 1h). The average numbers of primordial follicles per ovary were >1500 in *Tmco1*$^{+/+}$ and ~1000 in *Tmco1*$^{-/-}$ mice and primary follicles in KO ovaries were about three quarters of WT (Fig. 1i). Interestingly, corpora lutea (CL) were detectable in both genotypes (Fig. 1g, h), suggesting *Tmco1*$^{-/-}$ ovaries' own ovulation ability. Furthermore, aberrant follicle development turned obviously at 10 weeks. Compared with WT (Supplementary Figures S1L and M), only a few primordial follicles (arrows) were discovered in KO ovaries, indicating a diminished primordial follicle pool (Supplementary Figures S1N-P). At 16 weeks old, *Tmco1*$^{-/-}$ ovaries (Fig. 1j, k) exhibit substantially reduced numbers of all stages of ovarian follicles. The percentages of primary and secondary follicles were dramatically reduced (Fig. 1l) and could be scarcely found in *Tmco1*$^{-/-}$ ovaries (Fig. 1k, enlargement).

Tmco1 deletion causes POF in female mice

At 1-month old, degraded oocytes (Fig. 2a, b, arrows) were significantly piled up in KO ovaries, suggesting more prematurely active follicles underwent atresia (Fig. 2c). We then compared the total ovarian follicles from PD2 to PD157 and found a remarkable difference from PD4 to later on (Fig. 2d). The fact of *Tmco1* deletion leading to progressive loss of ovarian follicles implied *Tmco1* likely plays an important role in mouse ovarian follicle development. In addition, we measured serum hormone levels in mice aged around 16–22 weeks. The levels of FSH and LH (Fig. 2e, f) were elevated in *Tmco1*$^{-/-}$ mice, while estradiol (E2) was significantly decreased (Fig. 2g). Testosterone and progesterone (Fig. 2h, i) exhibited no obvious alterations. These phenotypes are analogous to POF of human patients.

To support that *Tmco1* depletion causes POF in *Tmco1*$^{-/-}$ mice, we further compared the ovarian and body weights of mice aged around 6–7 months. Both the ovarian and body weights in KO mice decreased to 80% of WT (Supplementary Figures S2A and B). However, the ratio of ovary weight to body weight was similar (Supplementary Figures S2C). Moreover, ovulated MII stage eggs of superovulating females (3-month-old) were fewer in *Tmco1*$^{-/-}$ mice (Supplementary Figure S2D). These data indicate *Tmco1* ablation may be one of the potential pathological causes of POF.

Deletion of *Tmco1* does not alter intracellular Ca^{2+} stores of GV oocytes and MII-arrested eggs

ER-mediated Ca^{2+} signaling is essential for oocytes maturation and follicle development [16]. Given that TMCO1 functions as a CLAC channel to maintain ER Ca^{2+} homeostasis in somatic cells [13], we speculated that the aberrant follicle development in *Tmco1* KO mice might be caused by increased ER Ca^{2+} level. To test it, ER Ca^{2+} levels of GV stage oocytes and MII eggs were compared. Surprisingly, we could not detect any obvious aberrance in Ca^{2+} store between WT and KO mice after 1 μM ionomycin (calcium ionophore) and 5 μM TG (thapsigargin) treatment, which specifically blocks the SR/ER Ca^{2+}-ATPase pumps (SERCA, Fig. 3) [17].

It is known that series of spontaneous Ca^{2+} oscillations are detected in GV oocytes after isolation from follicles and the oscillations may last for 2–3 h regardless of GVBD occurrence (germinal vesicle breakdown) [18, 19]. Interestingly, we observed altered spontaneous Ca^{2+} oscillations in *Tmco1*$^{-/-}$ GV oocytes, characterized by relative higher amplitude and lower frequency (Supplementary Figures S3A−C). In addition, the half-wave width (measurement of Ca^{2+} wave width at half maximum of amplitude) was significantly larger in GV oocytes of KO mice (Supplementary Figure S3D). Since GV oocytes were arrested in the prophase of first meiosis and acquire maturation when GVBD occurs [20], we then tested whether *Tmco1*$^{-/-}$ GV oocytes could resume meiosis during 1, 2, and 4 h after exposure to hCG. The result revealed no statistical difference of GVBD rate between two genotypes (Supplementary Figure S3K).

In fertilization, sperm–egg fusion induced Ca^{2+} release from ER, and Ca^{2+} wave triggered MII eggs to acquire resumption of meiotic cell division [21]. We next examined if *Tmco1* deletion would lead to altered Ca^{2+} response during fertilization. Zona-free MII eggs were inseminated with capacitated sperm of WT male mice with proven fecundity. The Ca^{2+} patterns were similar between WT and KO in vitro fertilization (Supplementary Figure S3E). Quantitative results manifested *Tmco1*$^{-/-}$ MII eggs had neither significant alterations in amplitude and duration of the first Ca^{2+} rise after sperm stimulation (Supplementary Figures S3F and G) nor in the following Ca^{2+} spikes (Supplementary Figures S3H and I). In addition, the numbers of Ca^{2+} peaks within the first hour did not vary either (Supplementary Figure S3J). Taken together, these results suggest depletion of *Tmco1* may not influence Ca^{2+} oscillations during in vitro fertilization.

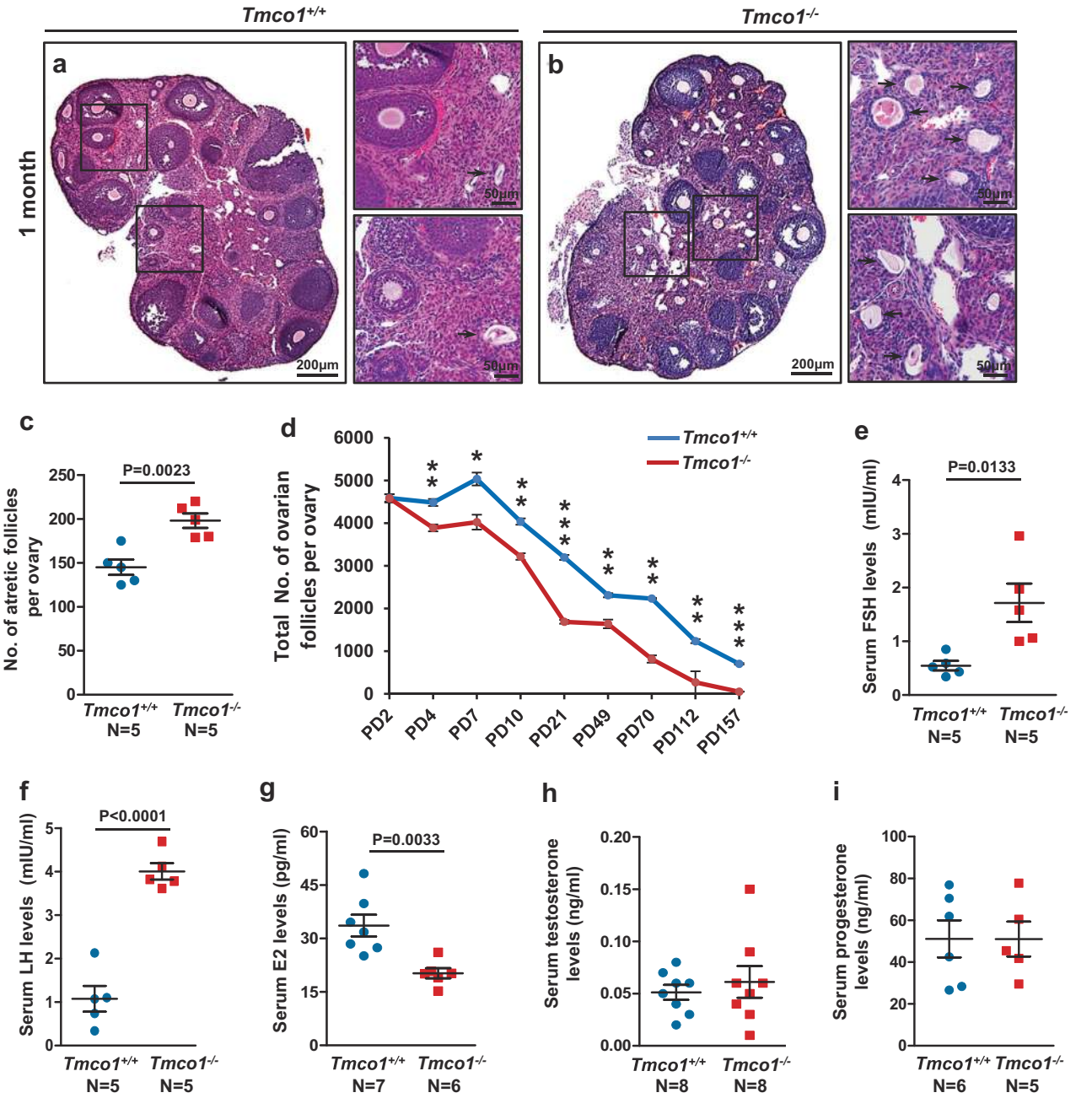

Fig. 2 Quantification of ovarian follicles and measurement of serum hormone levels. H&E staining of ovarian sections of 1-month-old **a** *Tmco1*$^{+/+}$ and **b** *Tmco1*$^{-/-}$ mice, arrows indicating the atretic follicles. Scale bars, 200 μm (**a**, **b**), 50 μm (enlargements). **c** More atretic follicles were counted in 1-month-old *Tmco1*$^{-/-}$ ovaries. **d** Total numbers of ovarian follicles in *Tmco1*$^{+/+}$ and *Tmco1*$^{-/-}$ mice from PD2 to PD157. At least five mice of each genotype for each time point were measured. PD4, $^{**}p = 0.0066$; PD7, $^{*}p = 0.0118$; PD10, $^{**}p = 0.0016$; PD21, $^{***}p < 0.0001$; PD49, $^{**}p = 0.0039$; PD70, $^{**}p = 0.0038$; PD112, $^{**}p = 0.0031$; PD157, $^{***}p = 0.0008$. **e**–**i** Sera collected from 16- to 22-week-old *Tmco1*$^{+/+}$ and *Tmco1*$^{-/-}$ mice were examined for hormone levels. Elevated levels of **e** FSH and **f** LH and **g** decreased E2 levels were observed in *Tmco1*$^{-/-}$ mice. **h** Testosterone and **i** progesterone levels had no significant difference

Increased intracellular Ca^{2+} stores in GCs isolated from *Tmco1*$^{-/-}$ ovaries

Given that GCs are the primary cell type in ovary that provides physical support and microenvironment required for developing oocytes [22], we examined whether the *Tmco1* deletion may bring about abnormal Ca^{2+} signaling and impaired ER calcium store in GCs. We collected GCs from PD23 ovaries after PMSG administration and found *Tmco1*$^{-/-}$ GCs manifested a supernormal Ca^{2+} signaling in

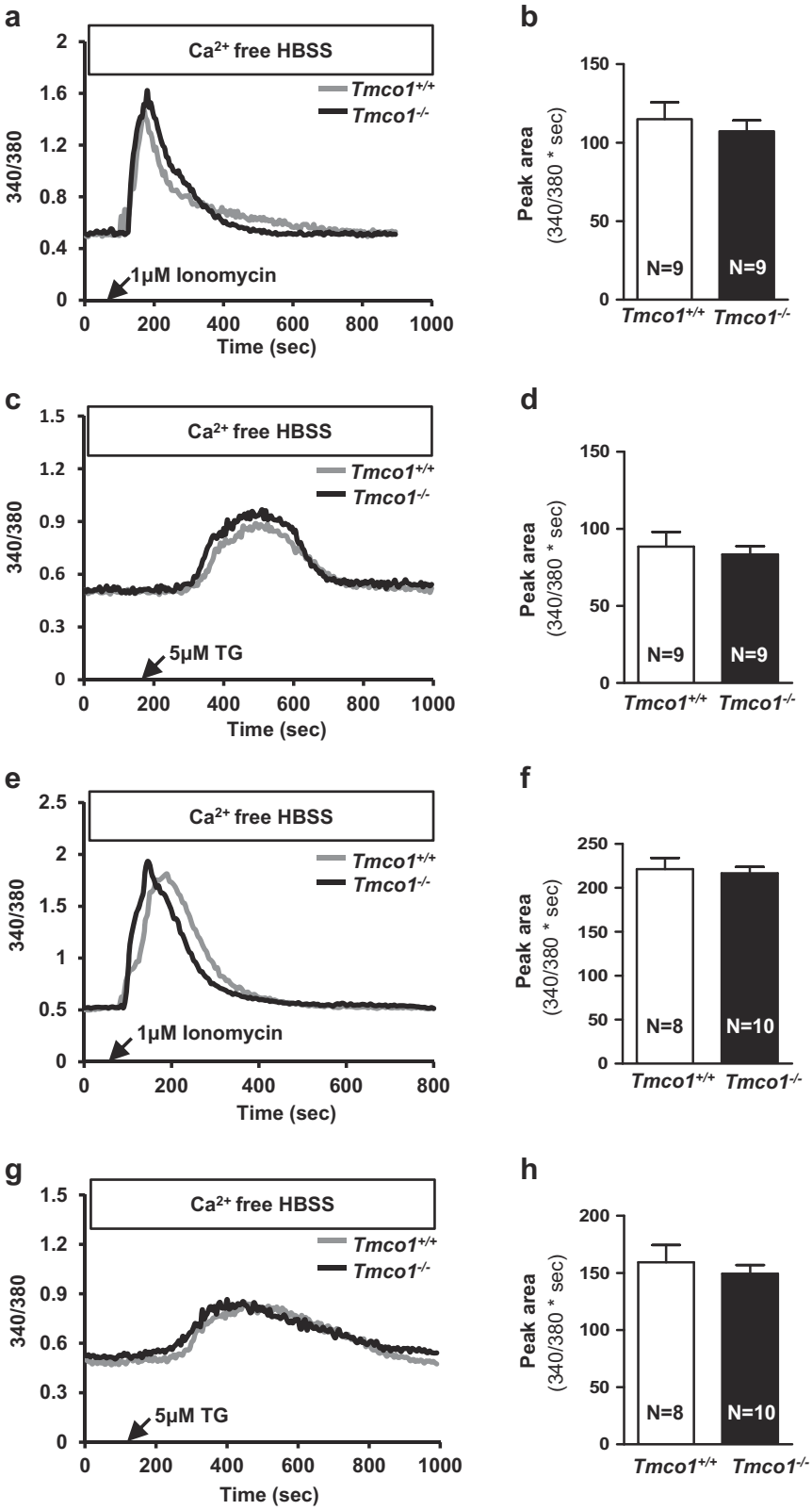

Fig. 3 Oocytes isolated from *Tmco1*$^{-/-}$ mice have normal Ca^{2+} signaling and ER Ca^{2+} storage. GV stage oocytes were collected from ovaries 48 h after PMSG injection in 23-day female mice. Black arrows indicated the time of treatment. **a** Ionomycin (1 μM) and **c** TG (5 μM)-triggered Ca^{2+} transients in Ca^{2+}-free HBSS. **b**, **d** Statistics summarized the average peak area of ionomycin and TG-stimulated Ca^{2+} mobilization. **e**–**h** Ca^{2+} signaling was normal in MII stage oocytes collected from oviductal ampullae of 4-week-old females after superovulation. Representative curves showed **e** Ionomycin (1 μM) and **g** TG (5 μM)-evoked the Ca^{2+} response. **f**, **h** Statistical analysis of the average peak area under ionomycin and TG-triggered Ca^{2+} mobilization curves of MII-arrested eggs

response to ionomycin (1 μM, Fig. 4a). The average peak area of Ca^{2+} transients was ~1.5-fold larger in KO GCs (Fig. 4b). Furthermore, TG also induced overactivation of Ca^{2+} signals in KO GCs with average area ~1.3 fold increase (Fig. 4c, d). Likewise, the Ca^{2+} storage evoked by 100 μM ATP was significantly larger in KO GCs (Fig. 4e, f).

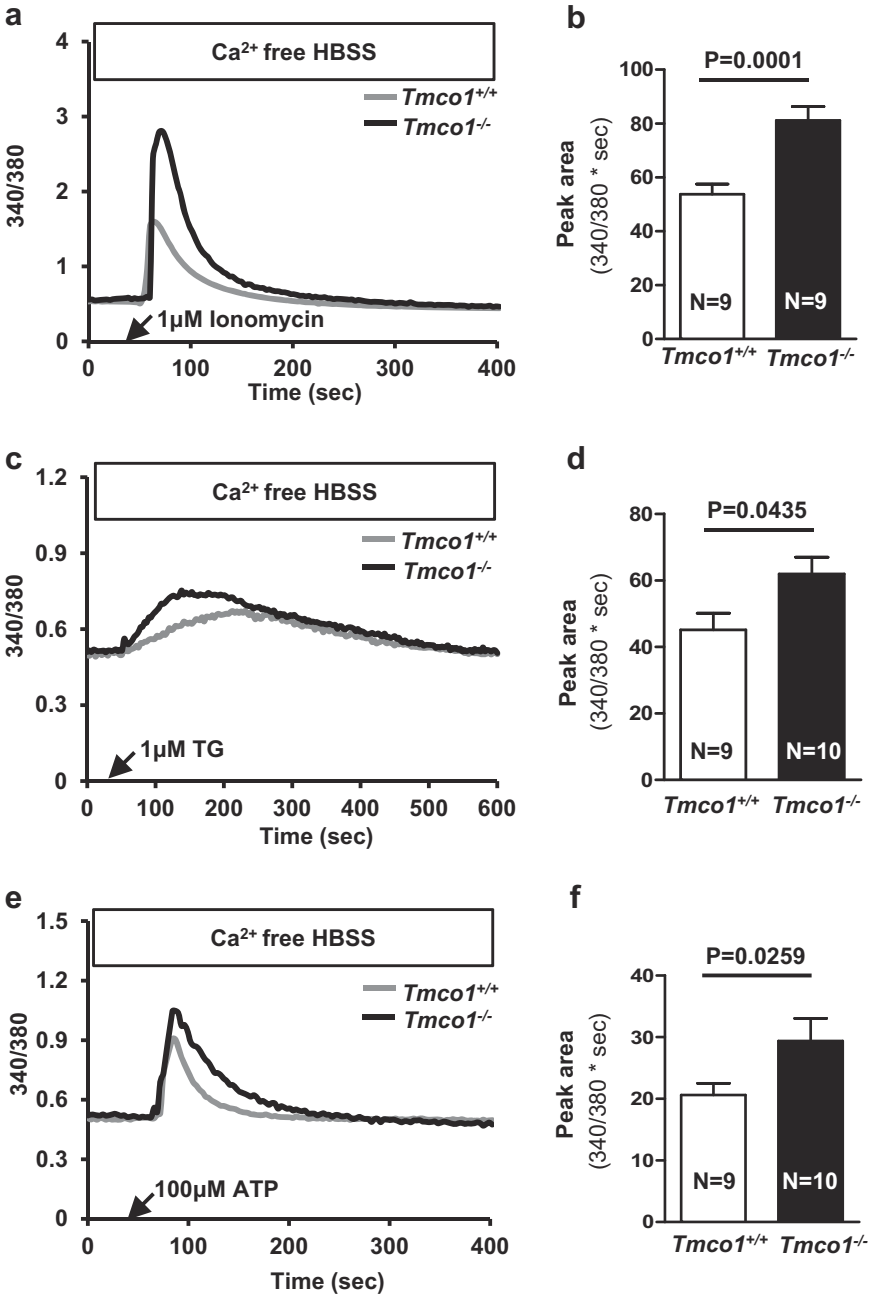

Fig. 4 *Tmco1* ablation results in abnormal Ca^{2+} signaling and ER Ca^{2+} overload in GCs. Black arrows indicated the time of treatment. **a** Ionomycin (1 μM)-evoked Ca^{2+} transients in primary GCs in Ca^{2+}-free medium. **b** Histogram of the average peak area of ionomycin-evoked Ca^{2+} transients in GCs. **c** TG (1 μM)-triggered Ca^{2+} signaling in GCs. **d** Bar chart presented the average of peak area of TG-induced Ca^{2+} transients. **e** Representative curves of ATP (100 μM)-stimulated Ca^{2+} response. **f** Summarized bar graph depicted much more elevation of Ca^{2+} mobilization induced by ATP in KO GCs

These data indicate TMCO1 is necessary in regulating ER Ca^{2+} store of mouse GCs and loss of TMCO1 function leads to overfilled ER Ca^{2+} store in *Tmco1*$^{-/-}$ GCs.

RNA-seq and IPA show altered diseases and functions in *Tmco1*$^{-/-}$ ovaries

To further understand how TMCO1 depletion affects follicle development, we collected PD7 ovaries for RNA-sequencing. The total numbers of reads generated from each sample varied from 34,529,346 to 64,837,339, which were aligned to the reference genome in an unique manner, with mapping rates between 85.43 and 86.95% (Supplementary Table S1). In total, at least 32,596 genes were expressed in WT and KO samples. Among them, 3060 significantly differentially expressed genes (DEGs) and 502 upregulated as well as 461 downregulated DEGs (fold change, FC > 1.5, KO/WT) were identified (Supplementary Tables S2 and 4). IPA (Ingenuity pathway analysis) was applied to investigate biological roles of the DEGs (Supplementary Table S5). Terms associated with calcium involving "Mobilization of Ca^{2+}", "Quantity of Ca^{2+}", and "Flux of Ca^{2+}" were

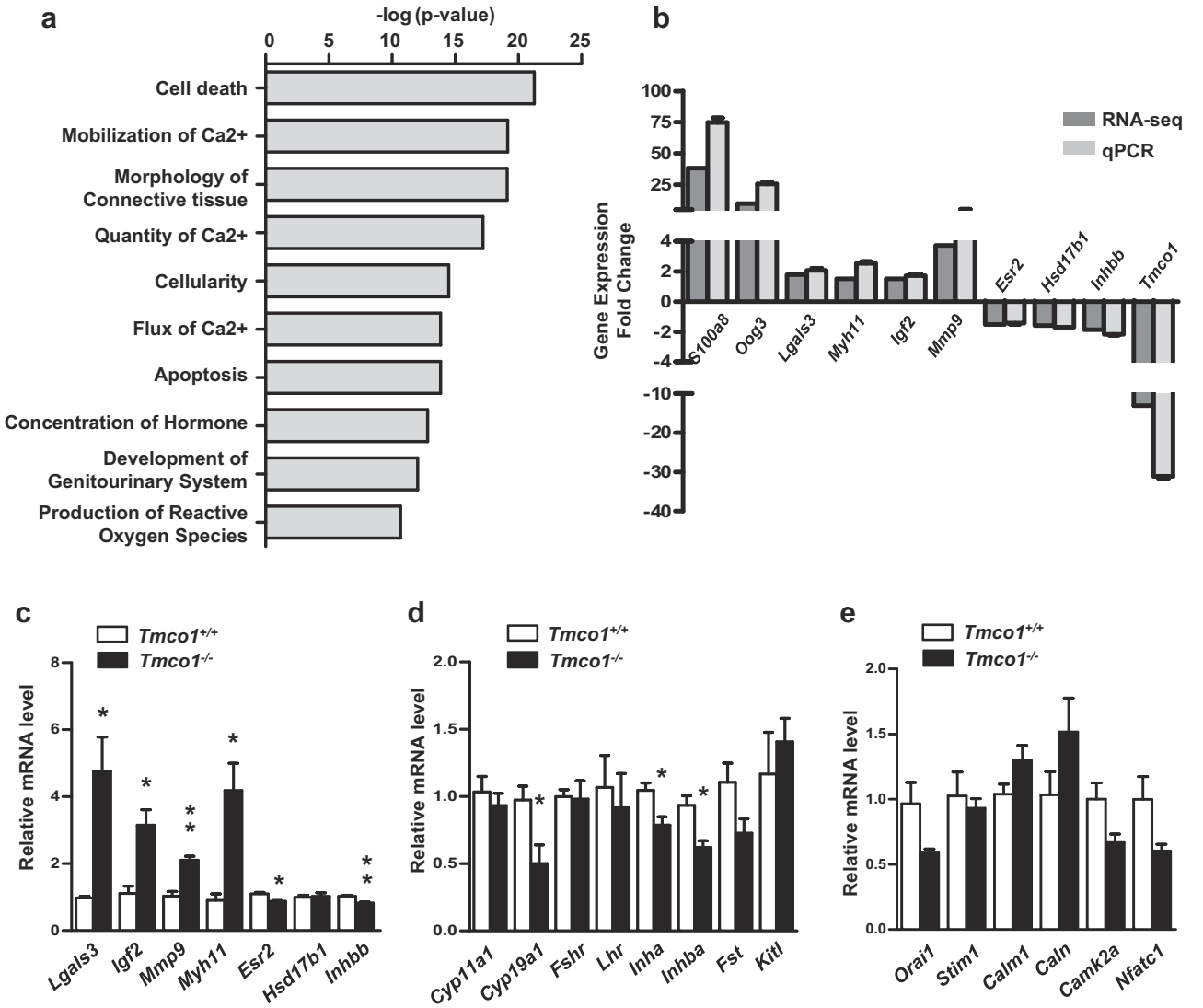

Fig. 5 RNA-seq and IPA show altered diseases and functions in *Tmco1*$^{-/-}$ ovaries. **a** Diseases and biological functions analysis of DEGs (FC > 1.5) identified by IPA. **b** qRT-PCR assays were used to validate the DEGs predicted by RNA-seq. RNA was isolated from 7-day-old mouse ovaries of *Tmco1*$^{+/+}$ ($N = 5$) and *Tmco1*$^{-/-}$ mice ($N = 5$). Six upregulated genes and four downregulated genes were determined and normalized by mouse *Gapdh* gene. **c**–**e** Relative mRNA levels were performed by qRT-PCR in GCs isolated from 23-day female mice after 48 h administration of PMSG ($N = 6$). **c** DEGs predicted by RNA-seq and **d** genes associated in follicular development as well as **e** calcium signaling were examined. The expression levels of *Lgals3* (*$p = 0.0208$), *Igf2* (*$p = 0.0163$), *Mmp9* (**$p = 0.0039$), and *Myh11*(*$p = 0.0169$) were significantly increased in *Tmco1*$^{-/-}$ GCs; nevertheless, the expression levels of *Esr2* (*$p = 0.0160$), *Inhbb* (**$p = 0.0049$), *Cyp19a1* (*$p = 0.0352$), *Inha* (*$p = 0.0337$) and *Inhba* (*$p = 0.0244$) were decreased in *Tmco1*$^{-/-}$ GCs

depicted as a network consisting of 32 genes, most of which had a positive function in Ca^{2+} homeostasis by annotated ingenuity relationships (Fig. 5a and Supplementary Figure S4A). In addition, terms of "Cell death" and "Apoptosis" were also enriched (Fig. 5a), indicating cell death is likely implicated in defective follicle development of *Tmco1*$^{-/-}$ mice. Moreover, *Igf2, Myh11, and Mmp9* were related to "Endoplasmic reticulum stress response" (Supplementary Figure S4B), suggesting ER stress response might affect the aberrant follicle development in *Tmco1*$^{-/-}$ ovaries. In particular, "Production of reactive oxygen species" indicated TMCO1 ablation might alter the ROS level in ovaries (Supplementary Figure S4C). Notably, genes enriched in "Concentration of hormone" manifested negative influence on regulation of hormone metabolism (Supplementary Figure S4D).

qRT-PCR was employed to confirm the validity of RNA-seq analysis. Six upregulated genes, including the top activated genes (*S100a8*, *Oog3*), ER stress-associated genes (*Myh11*, *Igf2*, *Mmp9*), and GCs apoptosis gene *Lgals3* as well as four downregulated genes in ovarian follicle development (*Esr2, Hsd17b1*, *Inhbb*) and *Tmco1* were

selected to amplify. These results indicated a good agreement between RNA-seq data and qRT-PCR (Fig. 5b).

In addition, we also extracted RNAs from the WT and KO GCs for qRT-PCR to confirm RNA-seq results (Fig. 5c). *Lgals3, Igf2, Mmp9, and, Myh11* were significantly increased in *Tmco1*$^{-/-}$ GCs, showing a well verification with RNA-seq analysis. The consistency was also qualified by repressed expression of *Inhbb* and *Esr2*. However, the mRNA level of *Hsd17b1*, which was downregulated in RNA-seq, did not change in *Tmco1*$^{-/-}$ GCs (Fig. 5c). Meanwhile, the mRNA levels of genes involved in follicular development and calcium signaling were determined. Expression levels of *Cyp19a1*, *Inha, and Inhba* were decreased in *Tmco1*$^{-/-}$ GCs (Fig. 5d). However, key receptors regulating follicle development like *Fshr* and *Lhr* did not alter. Nevertheless, the expression of genes participating in calcium signaling, such as *Orai1*, *Stim1*, *Calm1*, and *Caln*, was similar between WT and KO GCs (Fig. 5e).

Elevated ER stress-mediated apoptosis signaling and elevation of ROS levels in GCs isolated from *Tmco1*$^{-/-}$ ovaries

Consistent with ER stress response predicted by IPA, we noticed enhanced expressions of metabolic ER stress sensor inositol-requiring protein-1α (IRE1α) and activated phospo-IRE1 were significantly increased in *Tmco1*$^{-/-}$ GCs, which stimulated its downstream JNK (c-Jun N-terminal kinase) phosphorylation at Thr183/Tyr185 (Fig. 6a) and increased XBP1 splicing (Supplementary Figure S5B). However, levels of the known ER stress response pathways, protein kinase RNA (PKR)-like endoplasmic reticulum kinase (PERK), and activating transcription factor 6 (ATF6) cascade were similar in WT and KO GCs (Supplementary Figure S5A), supporting that loss of TMCO1 activates ER stress mainly mediated by activities of IRE1 pathway. In addition, TMCO1 depletion downregulated anti-apoptotic BCL2 expression and upregulated the levels of pro-apoptotic PUMA (p53 upregulated modulator of apoptosis) and BAX. During apoptosis, initiator procaspase 9 could be cleaved into active fragment and further processes the other executioner caspases, like caspase 3. Consistently, the levels of cleaved caspase 9 (CC9) and caspase 3 (CC3) were higher in *Tmco1*$^{-/-}$ GCs (Fig. 6a). Furthermore, we showed that *Tmco1*$^{-/-}$ GCs exhibited increased caspase 9 and caspase 3 activities (Supplementary Figure S5C, D), and enhanced IHC CC3 staining (Supplementary Figure S5E−G). The pan-caspase inhibitor Z-VAD-FMK could partially protect 3-week-old *Tmco1* KO mice from the loss of ovarian follicles (Supplementary Figure S6A−E) and partly suppress the apoptosis of GCs (Supplementary Figure S7A−E). These results indicate that TMCO1 ablation leads to elevated ER stress and apoptosis in GCs.

Since "Production of Reactive Oxygen Species" was also identified by IPA, we then assessed both intracellular and mitochondrial ROS levels in WT and KO GCs. As the main source of ROS in cell, mitochondrial ROS levels were determined using MitoSOX^{TM} Red probe (Fig. 6b). About 1.5-fold increase in the average fluorescence intensity was noticed in *Tmco1*$^{-/-}$ GCs (Fig. 6c). Furthermore, the intracellular ROS level, monitored by DCFH-DA probe, was also significantly elevated in *Tmco1*$^{-/-}$ GCs (Fig. 6d, e), supporting *Tmco1* deletion promotes ROS levels in GCs.

Deletion of *Tmco1* induces more ovarian follicles apoptosis of GCs

We next explored the extent of apoptosis in *Tmco1*$^{+/+}$ and *Tmco1*$^{-/-}$ ovaries by TUNEL method. Compared with WT ovaries (Fig. 6f, g), more TUNEL-positive primordial follicles, especially pregranulosa cells (Fig. 6h, i, arrows) and primary follicles (asterisks), were noticed in PD7 *Tmco1*$^{-/-}$ ovaries (Fig. 6j). In addition, abundant apoptotic GCs in secondary and early antral follicles were detected in PD21 KO ovaries (Fig. 6k–o).

Besides, the proliferation of GCs was also monitored. Ki67-positive GCs were observed in many secondary and early antral follicles (Supplementary Figures S8A and B, arrows) and no significant difference could be observed (Supplementary Figure S8C). These results indicate the loss of ovarian follicles in *Tmco1* mutant female mice is mostly associated with the apoptosis rather than proliferation of GCs.

Discussion

TMCO1 was recently reported to work as a CLAC channel [13], whose dysfunction results in human CFT dysplasia [15] and open angle glaucoma [23]. However, other physiological functions of TMCO1 in vivo remain unclear. In this study, we unexpectedly found that TMCO1 deletion caused subfertility in female mice, with a significant reduction of developing follicles and an increase of atretic follicles. *Tmco1*$^{-/-}$ mice exhibit a gradual loss of ovarian follicles since PD4, and no follicle structure at 6 months. Combined with the fact that the ovary size was reduced and serum levels of FSH and LH were elevated in *Tmco1*$^{-/-}$ mice, the POF phenotype in KO mice suggests that TMCO1 is necessary for ovarian follicle development and female fecundity.

POF is a heterogeneous disorder, which causes amenorrhea and ovarian failure of women before the age of 40 years [1]. The normal length of reproductive life and menopausal age in women are determined by the reserve of primordial follicles in the ovaries [24]. Deficiency of

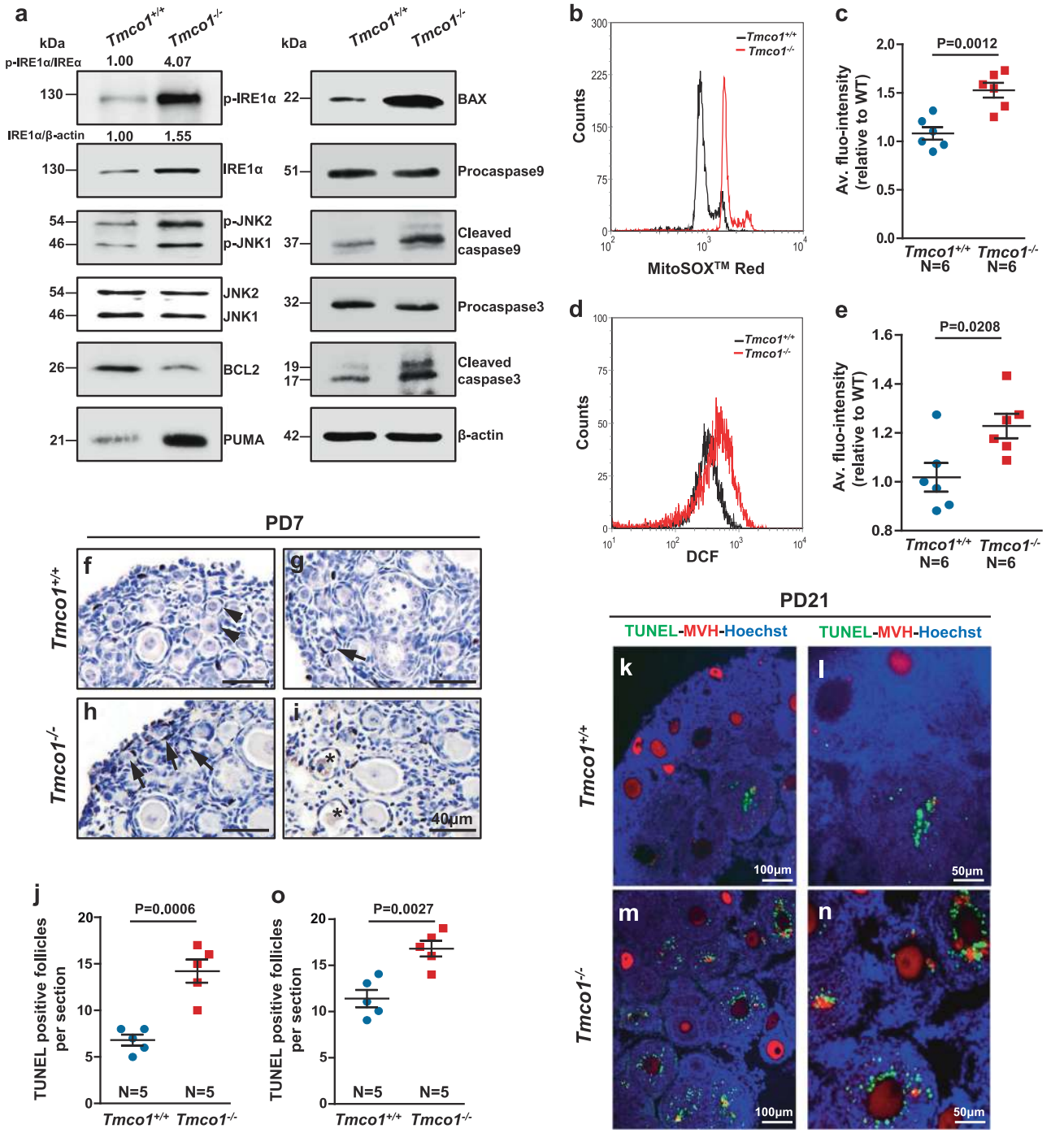

Fig. 6 Elevated ER stress-mediated apoptosis signaling and higher ROS levels in *Tmco1*$^{-/-}$ GCs. **a** Total protein extracted from the primary GCs were loaded and western blot tests were performed. Levels of β-actin were used as internal controls. **b**–**e** GCs were stained with MitoSOX™ Red probe (5 μM) or DCFH-DA probe (10 μM) to investigate mitochondrial ROS levels and intracellular ROS levels, respectively. Representative flow cytometry analyses illustrating **b** mitochondrial ROS levels and **d** intracellular ROS levels were shown in three independent experiments. **c**, **e** Statistical analysis summarized the average fluorescence intensity relative to control. Apoptosis of ovaries was assessed by TUNEL assay at **f**–**j** 7-day-old and **k**–**o** 21-day-old mice. **f**, **g** Normal primordial follicles (arrowheads) and fewer TUNEL-positive primordial follicles (arrows) were observed in 7-day control ovaries. **h**, **i** More TUNEL-positive primordial follicles (arrows) and primary follicles (asterisk) were noticed in 7-day *Tmco1*$^{-/-}$ ovaries. **j** Quantitive analysis of TUNEL-positive follicles of 7-day mice. **k**, **l** Few TUNEL-positive early antral follicles in ovaries of 21-day control mice. **m**, **n** TUNEL-positive GCs were frequently observed in both secondary follicles and early antral follicles. **l**, **n** Enlargement for (**k**, **m**). Green, TUNEL; red, MVH; blue, Hoechst. **o** Quantitive analysis of TUNEL-positive follicles of 21-day mice. Scale bars, 40 μm (**f**–**i**), 100 μm (**k**, **m**), 50 μm (**l**, **n**)

TMCO1 in mouse causes both premature depletion of primordial follicle pool and gradual loss of ovarian follicles of all stages, manifesting a typical etiology of POF in humans. In this sense, *Tmco1* KO mouse represents the pathogenesis of POF in humans and could be used as a mammalian model to study the molecular machinery underlying the premature loss of ovarian follicles in POF patients.

We previously reported that TMCO1 is capable of assembling into a Ca^{2+} channel to release Ca^{2+} from ER store when Ca^{2+} is overloaded [13]. Calcium signaling via GCs to oocytes is essential in meiosis resumption and maturation of oocytes [25, 26]. However, the relationship between Ca^{2+} homeostasis of GCs and oocytes towards ovarian follicle development is still elusive. To check whether TMCO1's function is conserved in ovarian cells that closely links with follicle development, we measured the levels of ER Ca^{2+} store in GCs and oocytes isolated from *Tmco1*$^{+/+}$ and *Tmco1*$^{-/-}$ mice. In accordance with the Ca^{2+} evoking pattern of osteoblasts cells from *Tmco1*$^{-/-}$ mice [13], we detected significantly enhanced Ca^{2+} signaling and ER Ca^{2+} store overloaded in KO GCs. Interestingly, GV stage oocytes and MII-arrested eggs did not show any obvious difference in ER Ca^{2+} store. One of the possible reasons might be unlike somatic cells, GV stage oocytes are arrested at diplotene stage of the first meiosis prophase [27] and MII eggs at metaphase of the second meiotic division. High levels of cyclic adenosine monophosphate (cAMP) lead to activation of protein kinase A, keeping oocytes from meiotic resumption [28]. To clarify this possibility, we added forskolin and IBMX, which could elevate cAMP levels [29, 30], into MEFs of WT and KO mice. The discrepancies of ratio area of ER Ca^{2+} store-evoked by TG became smaller (data not shown). Therefore, we speculate unlike overloaded ER Ca^{2+} store of somatic cells (GCs) of KO mice, *Tmco1* deletion may have different roles in oocytes in meiosis arrest.

Spontaneous calcium oscillations were exhibited during the meiosis resumption of immature GV stage mouse oocytes released from antral follicles [31]. We detected different Ca^{2+} patterns in *Tmco1*$^{-/-}$ GV oocytes, but GVBD rates of *Tmco1*$^{-/-}$ GV oocytes showed no obvious change after hCG administration, suggesting *Tmco1* deletion may not affect the maturation of GV oocytes in vitro. Fertilization-induced Ca^{2+} oscillation is a vital signal for activation of MII-arrested eggs to restore meiotic cell division [21]. In our study, sperm-evoke fertilization Ca^{2+} oscillations patterns were similar. Although with low fertility, *Tmco1*$^{-/-}$ female mice could still yield pups; therefore, TMCO1 is not likely to be necessary for fertilization process.

To elucidate how TMCO1 ablation affects follicle development, we performed RNA-seq analysis. Except for abnormal Ca^{2+} signaling, terms with enhanced cell death and apoptosis were enriched. We then detected several genes associated with ER stress. Overexpression of *Myh11*, for instance, has been reported in the activation of ER stress in smooth muscle cells [32]. In addition, genes with respect to apoptosis of GCs were also enriched. For instance, upregulated *Lgals3* [11] and downregulated *Inhbb* [12] by *Tmco1* ablation, indicating more apoptosis rate in KO GCs. Markedly declined concentration of serum estradiol of *Tmco1* KO mice could probably be attributed to decreased mRNA levels of *Cyp19a1*, which encodes the rate-limiting aromatase enzyme in estradiol production. *Esr2* is essential in folliculogenesis [33] and reduced fertility, including fewer pups and oocytes, following superovulation were observed in *Esr2* KO mice [34, 35]. In our study, *Esr2* mRNA level was significantly reduced in *Tmco1*$^{-/-}$ ovaries and GCs, which may result in subfertility of *Tmco1*$^{-/-}$ mice and reduced ovulated oocytes.

GCs secrete steroid and provide nutrients to oocyte for follicular growth. Moreover, GCs work as initiator of follicle atresia and underwent apoptosis during follicle degeneration, earlier than oocytes [9]. It is well established that prolonged abnormal ER calcium dynamics may severely affect the folding capacity of unfolded protein response (UPR) and trigger ER stress-associated mechanisms of cell death [36]. In *Tmco1*$^{-/-}$ ovaries, increased atretic follicles and more apoptotic ovarian follicles, especially apoptotic GCs were observed. Then, we explored whether supernormal Ca^{2+} signaling and elevated ER Ca^{2+} store would be associated with the apoptosis of *Tmco1*$^{-/-}$ GCs. As the most sensitive branch of UPR [37], IRE1α stimulates TRAF2 (tumor necrosis factor receptor associated factor 2), which then activates the ASK1 (apoptosis signal-regulating kinase 1) and forms IRE1α-TRAF2-ASK1 complex to phosphorylate and activate JNK [38]. We found IRE1α activation was higher and the level of BCL2 was reduced, while the levels of PUMA, BAX, cleaved caspase 9, and activated caspase 3 were increased in *Tmco1*$^{-/-}$ GCs. These results suggest elevated ER Ca^{2+} store in *Tmco1*$^{-/-}$ GCs causes ER stress-mediated GCs apoptosis, which then account for the gradual loss of ovarian follicles in *Tmco1* KO mice.

Chronic ER stress may result in impaired calcium release from the ER, increasing the production of mitochondrial ROS, which in turn further accelerate ER malfunction [39, 40]. ROS-induced oxidative stress can also cause severe impairment of ovarian follicle development, including rapid primordial follicle loss, GC apoptosis, large follicle atresia, and ovulated oocytes reduction [41, 42]. Consistently, we also detected elevated ROS levels in mitochondrial and intracellular in *Tmco1*$^{-/-}$ GCs.

It has been frequently noticed that genitourinary anomalies are the common clinical features of TMCO1-defect patients [14, 43], suggesting that normal function of

TMCO1 is important for the development of genital urinary system. However, ovarian function had not been examined in the female clients, so it is not known if TMCO1-defect patients have defects in ovarian function. By exploring the currently available database resource, there is no direct association between POF and *Tmco1* mutations. Nevertheless, *Tmco1* gene mutations that partially disable TMCO1's function could be the risk factor for human POF. Further analysis of *Tmco1* sequence in large cohorts of POF patients will provide a great opportunity to identify causative mutation(s), which will be potentially useful for future diagnostic/prognostic purposes.

In summary, we reveal for the first time that *Tmco1* is required for ovarian follicle development, which is closely linked with the role of TMCO1 in maintaining normal ER Ca^{2+} store in GCs. Deletion of *Tmco1* can cause ER Ca^{2+} overloaded in GCs followed by ER stress and oxidative stress. Accordingly, more GCs undergo apoptosis, resulting in more atretic follicles and gradual but rapid loss of follicles in $Tmco1^{-/-}$ mice. Our results not only shed new light on the role of *Tmco1* in ovarian physiology and pathology but also extend our understanding of potential genes associated with POF in human patients.

Materials and methods

Mice

The $Tmco1^{+/-}$ mouse strain (C57BL/6J) was generated in Shanghai Model Organisms Center, Inc. (Shanghai, China). Briefly, a *Tmco1* targeting vector, which was constructed by ET cloning techniques in EL250 bacterial cells [44], was designed to replace a 1.01-kb fragment with a pGK-Neomycin-polyA cassette. The replaced 1.01-kb fragment contains the coding region of exons 1 and 2. The targeting vector was electroporated into a mouse embryonic stem cell (ES) line with C57BL/6J*129S3 background. After double drug selection with G418 and GANC, the resistant ES clones were identified by long PCR and confirmed by sequencing. Positive ES cell clones were expanded and injected into C57BL/6J blastocysts to generate the chimeric offspring. The chimeric mice were mated with C57BL/6J mice to obtain the *Tmco1* heterozygous mice, which were then backcrossed to C57BL/6J for six generations before the experiment. DNAs obtained from tail and toe biopsies were used for genotyping with the following primers:

ARM sense:5′-AGGTAACGCACTGCCGAGGT-3′;
intron anti:5′-CAGTGCCCTTCCACCCTGGG-3′;
Neo anti:5′-GAGATCCTGCCCCGGCACTTC-3′.

The mice were housed in cages under a 12/12 h light/dark cycle. All the animal procedures were reviewed and approved by the Institute of Zoology, Institutional Animal Care and Use Committee and were conducted according to the committee's guidelines.

Fertility assay

Seven-week-old *Tmco1* KO and WT female mice were housed with WT C57BL/6J males (2–3-month-old), which were proved having normal fecundity. Copulatory plugs were monitored daily, and plugged females with visibly growing abdomen were moved to separate cages for monitoring pregnancy. The mating process lasted for 4.5 months. The numbers of pups (both alive and dead) were counted on the first day of life.

Histological analysis

Ovaries were fixed in 4% paraformaldehyde, dehydrated in graded ethanol and embedded in paraffin. Serial sections (5 μm) were prepared for hematoxylin−eosin (HE) staining and immunohistochemistry (IHC) analysis. MVH (Vasa), a germ cell marker, was used to identify the oocytes. The primary antibodies used for IHC analysis were as follows: anti-DDX4/MVH (1:1000, Abcam, ab13840), anti-Ki67 (1:200, Abcam, ab15580), and anti-cleaved caspase 3 (1:300, CST, 9661). Biotinylated anti-rabbit IgG (H + L) (1:200, ZSGB-BIO, ZB-2010) was used as secondary antibody. Horseradish peroxidase Streptavidin (1:200, ZSGB-BIO, ZB-2404) and DAB substrate (ZLI-9017, ZSGB-BIO) were then employed and sections were counterstained with hematoxylin. Every fifth serial section was analyzed by light microscopy for the presence of primordial, primary, secondary and early antral and antral follicles based on morphological classification of mouse follicles [45]. Images were captured by an automated multispectral Vectra™ imaging system (Perkin Elmer Vectra™, Waltham, MA).

Serum hormone measurement

Adult $Tmco1^{-/-}$ female mice aged around 16−22 weeks were killed because of irregular estrus cycles; WT female mice at the same age were killed at the proestrus stage (by investigating the pudendum appearance) to avoid the ovulation phase. Blood was collected by removing an eyeball. The serum was separated and stored at −80 °C until use. Levels of serum FSH, LH, estradiol (E2), progesterone, and testosterone were measured using a radioimmunoassay in Beifang Institute of Biological Technology (Beijing, China).

Superovulation and collection of oocytes

Female mice at 23 days of age were killed by cervical dislocation 48 h after i.p. injection with pregnant mare serum gonadotrophin (PMSG, 7 IU). Ovaries were

dissected and repeatedly punctured in M2 medium (Sigma, M7167). Cumulus-oocyte complexes were released from antral follicles. Denuded oocytes with intact zona pellucida and clear nuclear membrane were collected as GV stage oocytes, which were then cultured in M16 medium (Sigma, M7292) covered by mineral oil (Sigma, M8410). To avoid spontaneous maturation of GV oocytes, dbcAMP (0.1 mg/ml, Sigma, D2060) was added in the medium. Four-week-old female mice were injected i.p. with 7 IU human chorionic gonadotropin (hCG) 48 h after injection of 7 IU PMSG. Mice were killed 13 h after hCG injection. MII eggs and cumulus cells complex were collected from oviducts. After hyaluronidase (1 mg/ml, Sigma, H4272) treatment, cumulus mass was dissociated and MII eggs were collected in M16 medium. For in vitro fertilization experiment, zona pellucidae were removed by brief treatment with acid tyrode solution (Sigma, T1788) and eggs were washed thoroughly in human tubal fluid (HTF, Merck Millipore, MR-070-D). Cauda epididymal sperm were collected from 3-month-old WT male mice with proved fecundity and capacitated in HTF medium for 1 h at 37 °C incubator with 5% CO_2. Each MII egg was allowed to bind 3–4 sperm to prevent the chance of polyspermy [19].

Granulosa cells isolation

Female mice at 23 days of age were killed by cervical dislocation 48 h after injection with PMSG (7 IU). Ovaries were dissected and large antral follicles were punctured in M2 medium to extrude GCs which were then harvested. One part of GCs were mixed with SDS loading buffer and boiled for 10 min at 100 °C for SDS-PAGE. Other part GCs were cultured in DMEM/F12 medium complemented with 5% FBS, 100 IU/ml penicillin, and 100 mg/ml streptomycin sulfate shortly for use [10].

Ca^{2+} imaging

Ca^{2+} imaging assay was performed as described previously [13]. Fura2-AM was used as a ratiometric indicator of cellular calcium concentrations, which were assessed according to 340/380 ratio by fluorescence. Isolated oocytes and GCs were loaded with 4 μM calcium indicator Fura2-AM (Invitrogen, F1221) and 0.1% pluronic F-127 (Invitrogen, P3000MP) in HBSS for 40 min at 37 °C. After several rinses, cells were attached to polylysine-coated confocal dishes for measurement. HBSS-Ca^{2+}-free solutions containing 1 mM EGTA were applied to evaluate the intracellular Ca^{2+} store out of the presence of extracellular Ca^{2+} uptake. Thapsigargin (TG, Sigma, T9033), a specific inhibitor of the ER Ca^{2+}-ATPase, was adopted 5 μM for oocytes and 1 μM for GCs to measure the ER Ca^{2+} store. For other experiments, 1 μM ionomycin (Sigma) and 100 μM ATP (MP biochemical) were used to monitor the intracellular Ca^{2+} store. For evaluation of Ca^{2+} oscillations during in vitro fertilization, imaging began immediately after adding capacitated sperm to chambers maintained at 37 °C by a thermostatic controller. Images were recorded every 2–5 s under a Nikon inverted microscope (Eclipse Ti) with ×20 objective for oocytes and ×40 oil-immersing objective for GCs. Ratio of Fura-2 fluorescence images was captured with alternatively excitation filters of 340 and 380 nm and processed through Metamorph software (version 7.0). Data analysis was carried out using Excel (2010) and GraphPad Prism software (version 5.0).

RNA isolation and real-time PCR

Total RNAs from either 7-day ovaries or isolated GCs were extracted by using Trizol Reagent (Invitrogen, 15596026). The cDNAs were synthesized by using GoStript™ Reverse Transcription System (Promega, A5001). Quantitative real-time PCR reactions for target genes were performed using SYBR Green Real-time PCR Master Mix (TOYOBO, QPK-201). Target genes expression levels were calculated in comparative Ct ($\triangle\triangle$Ct) value method and normalized against glyceraldehyde-3-phosphate dehydrogenase (*Gapdh*). For *Xbp1* mRNA splicing analysis, total RNAs were obtained from GCs of 23-day female mice after superovulation as described above. The extent of *XBP1* splicing was determined by RT-PCR. Primers used for real-time PCR and *Xbp1* mRNA splicing analysis were listed in Supplementary Table S3. The experiments were performed in triplicate.

RNA sequencing

Ovarian total RNAs were isolated from 7-day-old mice by using Trizol Reagent. Four groups (WT-1, WT-2, KO-1, and KO-2) of ovarian RNAs (ten ovaries from five mice for each group) were applied for RNA-sequencing. The sequencing libraries were prepared following the manufacturer's instructions (Illumina). The integrity of RNA was assessed on Bioanalyzer (Agilent Technologies 2100). Approximately 1 μg total RNA was applied to cDNA libraries preparation for sequencing. Briefly, Poly-T oligo-attached magnetic beads were used to isolate poly-adenylated RNA (Stranded mRNA-seq Kit Illumina platform, KAPA, KK8441). The extracted mRNA was fragmented and cDNA was synthesized according to the manufacturer's instructions (Stranded RNA-Seq kit, KAPA, KK8401). RNA-seq libraries were assessed by using a DNA 1000 kit of the Bioanalyzer 2100 system (Agilent Technologies, 5067-1504). Libraries were pooled and sequencing was carried out on an Illumina HiSeq 3000 with paired-end, 100 bp read length.

Differential expression analysis

RNA-seq data were aligned to the mouse genome (mm10) using Tophat (v2.1.0). Differential genes expression analysis was compared through edgeR (3.8.6). The genes on the basis of a P value < 0.05 and fold change >1.5 were described as differentially expressed.

Differentially expressed genes function analysis

The diseases and biological functions analysis was determined using IPA (Winter Release 2016, version 31813283). Ensemble accession of DEGs was used as the identifier.

Western blot analysis

Total protein was extracted from GCs, oocytes, and ovaries using RIPA buffer (Solarbio, R0020, China). Protein concentration was assessed by BCA assay (Cellchip, China). Protein extracts separated by SDS-PAGE were blotted with the following primary antibodies: anti-IRE1α (1:1000, CST, 3294), anti-phospho-IRE1 (Ser724, 1:1000, Abcam, ab48187), anti-Bcl2 (1:500, Proteintech, 12789-1-AP), anti-Bax (1:500, Ruiying, RLT0456), anti-JNK (1:500, Proteintech, 51151-1-AP), anti-phospho-JNK (Thr183/Tyr185, 1:1000, CST, 4688), anti-caspase 9 (1:1000, CST, 9508), anti-cleaved caspase 9 (1:1000, CST, 9509) anti-caspase 3, (1:700, Proteintech, 19677-1-AP), anti-cleaved caspase 3 (1:1000, CST, 9661), anti-XBP1 (1:400, Santa Cruz, sc8015), anti-ATF6 (1:400, Santa Cruz, sc166659), anti-BiP/GRP78 (1:1000, Santa Cruz, sc376768), anti-phospho-PERK (Thr980, 1:1000, CST, 3179), anti-PERK (1:1000, CST, 3192), anti-phospho-eIF2α (Ser51, 1:1000, CST, 3398), anti-eIF2α (1:1000, CST, 9722), anti-ATF4 (1:1000, CST, 11815), anti-CHOP (1:500, Proteintech, 15204-1-AP), and TMCO1 antibody (1:1000) [13].

TUNEL assay

Terminal deoxynucleotidyl transferase nick end labeling (TUNEL) assays were performed to evaluate cell apoptosis of follicles using 5 μm paraffin-embedded sections, according to the manufacturer's instructions of In Situ Cell Death Detection Kit, POD (Roche, Cat. No.11684817910). For light microscopy, DAB substrate was added and sections were counterstained with hematoxylin. TUNEL-positive cells had dark brown nuclei indicating apoptosis. For fluorescence microscopy, sections marked with germ cells using anti-DDX4/MVH (1:1000, Abcam, ab13840) and TUNEL signal acquired excitation wavelength in the 490 nm and detection in 525 nm.

ROS detection analysis

Intracellular ROS levels were analyzed using Reactive Oxygen Species Assay Kit (Beyotime, S0033, China) according to the manufacturer's instruction. GCs were isolated and suspended in diluted DCFH-DA, an oxidation-sensitive fluorescent probe, and incubated at 37 °C for 20 min in 5% CO_2. After washing with serum-free medium, cell fluorescence was immediately detected at excitation (488 nm) and emission (525 nm) wavelengths by flow cytometry analysis. MitoSOX^{TM} Red (Invitrogen, M36008) was applied to measure the ROS levels in mitochondria. GCs were loaded with probe for 10 min at 37 °C and washed using HBSS. Cell fluorescence was observed at excitation (510 nm) and emission (580 nm) by flow cytometry analysis.

Caspase activity assays

The protein concentrations of GCs were quantified using Bradford protein quantification method (P0006, Beyotime, China). Caspase 3 activity (C1115, Beyotime, China) and caspase 9 activity (C1157, Beyotime, China) were detected according to the instructions. Absorbance at 405 nm was detected using a microplate reader.

Statistical analysis

All experiments were repeated at least three times. Statistical analyses were performed using Prism (version 5.0, GraphPad Software, Inc., La Jolla, CA, USA). Data were presented as mean ± s.e.m. and significant differences between groups were calculated with two-tailed Student's t test. Differences were considered significant at $^{*}P < 0.05$, $^{**}P < 0.01$, and $^{***}P < 0.001$.

Data availability

The sequence data reported in this paper have been deposited in the Genome Sequence Archive [46] (http://bigd.big.ac.cn/gsa/) in BIG Data Center [47], Beijing Institute of Genomics (BIG), Chinese Academy of Sciences, under accession number CRA000296. The data supporting the findings of this study are available from the corresponding authors upon request.

Acknowledgements This work was supported by National Key Research and Development Program of China 2017YFC1001001, NSFC91754204, 81630078, 31471331, 31670822, 81371415, and 31570816, CAS Strategic Priority Research Program XDA16010107 and XDB14030300, the State Key Laboratory of Membrane Biology and CAS Key Laboratory of Genomic and Precision Medicine.

Author contributions Z.S. performed most of the experiments, H.Z. performed qRT-PCR, X.W. and Q.-C.W. performed Ca^{2+} imaging measurement, C.Z. and H.Z. analyzed RNA-seq data and performed DEG analysis, Y.-H.W. and J.-Q.W. assisted in immunofluorescence imaging, C.-Q.A. assisted in sera collection, K.-Y.Y. and Y.W. assisted in mice breeding, F.G. and T.-S.T. guided follicle development analysis, T.-S.T. and C.G. designed the whole project, Z.S., T.-S.T. and C.G. analyzed the data and wrote the manuscript with input from all authors.

Compliance with ethical standards

Conflict of interest The authors declare that they have no conflict of interest.

References

1. Pouresmaeili F, Fazeli Z. Premature ovarian failure: a critical condition in the reproductive potential with various genetic causes. Int J Fertil Steril. 2014;8:1–12.
2. Devi A, Benn PA. X-chromosome abnormalities in women with premature ovarian failure. J Reprod Med. 1999;44:321–4.
3. Bodega B, Bione S, Dalpra L, Toniolo D, Ornaghi F, Vegetti W, et al. Influence of intermediate and uninterrupted FMR1 CGG expansions in premature ovarian failure manifestation. Hum Reprod. 2006;21:952–7.
4. Reddy P, Liu L, Adhikari D, Jagarlamudi K, Rajareddy S, Shen Y, et al. Oocyte-specific deletion of Pten causes premature activation of the primordial follicle pool. Science. 2008;319:611–3.
5. Reddy P, Adhikari D, Zheng W, Liang S, Hamalainen T, Tohonen V, et al. PDK1 signaling in oocytes controls reproductive aging and lifespan by manipulating the survival of primordial follicles. Hum Mol Genet. 2009;18:2813–24.
6. Sobinoff AP, Sutherland JM, McLaughlin EA. Intracellular signalling during female gametogenesis. Mol Hum Reprod. 2013;19:265–78.
7. Ikami K, Nuzhat N, Lei L. Organelle transport during mouse oocyte differentiation in germline cysts. Curr Opin Cell Biol. 2017;44:14–19.
8. Dumesic DA, Meldrum DR, Katz-Jaffe MG, Krisher RL, Schoolcraft WB. Oocyte environment: follicular fluid and cumulus cells are critical for oocyte health. Fertil Steril. 2015;103:303–16.
9. Matsuda F, Inoue N, Manabe N, Ohkura S. Follicular growth and atresia in mammalian ovaries: regulation by survival and death of granulosa cells. J Reprod Dev. 2012;58:44–50.
10. Gao F, Zhang J, Wang X, Yang J, Chen D, Huff V, et al. Wt1 functions in ovarian follicle development by regulating granulosa cell differentiation. Hum Mol Genet. 2014;23:333–41.
11. Lohr M, Kaltner H, Lensch M, Andre S, Sinowatz F, Gabius HJ. Cell-type-specific expression of murine multifunctional galectin-3 and its association with follicular atresia/luteolysis in contrast to pro-apoptotic galectins-1 and -7. Histochem Cell Biol. 2008;130:567–81.
12. M'Baye M, Hua G, Khan HA, Yang L. RNAi-mediated knockdown of INHBB increases apoptosis and inhibits steroidogenesis in mouse granulosa cells. J Reprod Dev. 2015;61:391–7.
13. Wang QC, Zheng Q, Tan H, Zhang B, Li X, Yang Y, et al. TMCO1 is an ER Ca(2+) load-activated Ca(2+) channel. Cell. 2016;165:1454–66.
14. Xin B, Puffenberger EG, Turben S, Tan H, Zhou A, Wang H. Homozygous frameshift mutation in TMCO1 causes a syndrome with craniofacial dysmorphism, skeletal anomalies, and mental retardation. Proc Natl Acad Sci USA. 2010;107:258–63.
15. Alanay Y, Erguner B, Utine E, Hacariz O, Kiper PO, Taskiran EZ, et al. TMCO1 deficiency causes autosomal recessive cerebrofaciothoracic dysplasia. Am J Med Genet A. 2014;164A:291–304.
16. Mann JS, Lowther KM, Mehlmann LM. Reorganization of the endoplasmic reticulum and development of Ca2+release mechanisms during meiotic maturation of human oocytes. Biol Reprod. 2010;83:578–83.
17. Thastrup O, Cullen PJ, Drobak BK, Hanley MR, Dawson AP. Thapsigargin, a tumor promoter, discharges intracellular Ca2+stores by specific inhibition of the endoplasmic reticulum Ca2(+)-ATPase. Proc Natl Acad Sci USA. 1990;87:2466–70.
18. Carroll J, Swann K. Spontaneous cytosolic calcium oscillations driven by inositol trisphosphate occur during in vitro maturation of mouse oocytes. J Biol Chem. 1992;267:11196–201.
19. Deng MQ, Huang XY, Tang TS, Sun FZ. Spontaneous and fertilization-induced Ca2+oscillations in mouse immature germinal vesicle-stage oocytes. Biol Reprod. 1998;58:807–13.
20. Sun QY, Miao YL, Schatten H. Towards a new understanding on the regulation of mammalian oocyte meiosis resumption. Cell Cycle. 2009;8:2741–7.
21. Miyazaki S, Ito M. Calcium signals for egg activation in mammals. J Pharmacol Sci. 2006;100:545–52.
22. Huang Z, Wells D. The human oocyte and cumulus cells relationship: new insights from the cumulus cell transcriptome. Mol Hum Reprod. 2010;16:715–25.
23. Burdon KP, Macgregor S, Hewitt AW, Sharma S, Chidlow G, Mills RA, et al. Genome-wide association study identifies susceptibility loci for open angle glaucoma at TMCO1 and CDKN2B-AS1. Nat Genet. 2011;43:574–8.
24. Adhikari D, Liu K. Molecular mechanisms underlying the activation of mammalian primordial follicles. Endocr Rev. 2009;30:438–64.
25. Wang C, Machaty Z. Calcium influx in mammalian eggs. Reproduction. 2013;145:R97–R105.
26. Silvestre F, Boni R, Fissore RA, Tosti E. Ca2+signaling during maturation of cumulus-oocyte complex in mammals. Mol Reprod Dev. 2011;78:744–56.
27. Borum K. Oogenesis in the mouse. A study of the origin of the mature ova. Exp Cell Res. 1967;45:39–47.
28. Bornslaeger EA, Mattei P, Schultz RM. Involvement of cAMP-dependent protein kinase and protein phosphorylation in regulation of mouse oocyte maturation. Dev Biol. 1986;114:453–62.
29. Urner F, Herrmann WL, Baulieu EE, Schorderet-Slatkine S. Inhibition of denuded mouse oocyte meiotic maturation by forskolin, an activator of adenylate cyclase. Endocrinology. 1983;113:1170–2.

30. Yoon SY, Choe C, Kim EJ, Kim CW, Han J, Kang D. Acetylcholine controls mouse oocyte maturation via downregulation of cAMP. Clin Exp Pharmacol Physiol. 2011;38:435–7.
31. Carroll J, Swann K, Whittingham D, Whitaker M. Spatiotemporal dynamics of intracellular [Ca2+]i oscillations during the growth and meiotic maturation of mouse oocytes. Development. 1994;120:3507–17.
32. Kwartler CS, Chen J, Thakur D, Li S, Baskin K, Wang S, et al. Overexpression of smooth muscle myosin heavy chain leads to activation of the unfolded protein response and autophagic turnover of thick filament-associated proteins in vascular smooth muscle cells. J Biol Chem. 2014;289:14075–88.
33. Drummond AE, Fuller PJ. The importance of ERbeta signalling in the ovary. J Endocrinol. 2010;205:15–23.
34. Couse JF, Curtis Hewitt S, Korach KS. Receptor null mice reveal contrasting roles for estrogen receptor alpha and beta in reproductive tissues. J Steroid Biochem Mol Biol. 2000;74:287–96.
35. Couse JF, Yates MM, Deroo BJ, Korach KS. Estrogen receptor-beta is critical to granulosa cell differentiation and the ovulatory response to gonadotropins. Endocrinology. 2005;146:3247–62.
36. Sano R, Reed JC. ER stress-induced cell death mechanisms. Biochim Biophys Acta. 2013;1833:3460–70.
37. Wu J, He GT, Zhang WJ, Xu J, Huang QB. IRE1alpha signaling pathways involv1ed in mammalian cell fate determination. Cell Physiol Biochem. 2016;38:847–58.
38. Zeng T, Peng L, Chao H, Xi H, Fu B, Wang Y, et al. IRE1alpha-TRAF2-ASK1 complex-mediated endoplasmic reticulum stress and mitochondrial dysfunction contribute to CXC195-induced apoptosis in human bladder carcinoma T24 cells. Biochem Biophys Res Commun. 2015;460:530–6.
39. Chaudhari N, Talwar P, Parimisetty A, Lefebvre d'Hellencourt C, Ravanan P. A molecular web: endoplasmic reticulum stress, inflammation, and oxidative stress. Front Cell Neurosci. 2014;8:213.
40. Cao SS, Kaufman RJ. Endoplasmic reticulum stress and oxidative stress in cell fate decision and human disease. Antioxid Redox Signal. 2014;21:396–413.
41. Devine PJ, Perreault SD, Luderer U. Roles of reactive oxygen species and antioxidants in ovarian toxicity. Biol Reprod. 2012;86:27.
42. Zhang JQ, Shen M, Zhu CC, Yu FX, Liu ZQ, Ally N, et al. 3-Nitropropionic acid induces ovarian oxidative stress and impairs follicle in mouse. PLoS ONE. 2014;9:e86589.
43. Pehlivan D, Karaca E, Aydin H, Beck CR, Gambin T, Muzny DM, et al. Whole-exome sequencing links TMCO1 defect syndrome with cerebro-facio-thoracic dysplasia. Eur J Hum Genet. 2014;22:1145–8.
44. Liu P, Jenkins NA, Copeland NG. A highly efficient recombineering-based method for generating conditional knockout mutations. Genome Res. 2003;13:476–84.
45. Myers M, Britt KL, Wreford NG, Ebling FJ, Kerr JB. Methods for quantifying follicular numbers within the mouse ovary. Reproduction. 2004;127:569–80.
46. Wang Y, Song F, Zhu J, Zhang S, Yang Y, Chen T, et al. GSA: Genome Sequence Archive. Genom Proteom Bioinforma. 2017;15:14–18.
47. Members BIGDC. The BIG Data Center: from deposition to integration to translation. Nucleic Acids Res. 2017;45:D18–D24.